Doping silica beyond limits with laser plasma for active photonic materials

Jayakrishnan Chandrappan,[1*] Matthew Murray,[1] Peter Petrik,[2] Emil Agocs,[2] Zsolt Zolnai,[2] Agnès Tempez,[3] Sébastien Legendre,[3] D. P. Steenson,[4] Animesh Jha,[1] and Gin Jose[1]

[1]*Institute for Materials Research, School of Chemical and Process Engineering, Faculty of Engineering, University of Leeds, LS2 9JT, UK*
[2]*Institute of Technical Physics and Materials Science, Hungarian Academy of Sciences, 1121 Budapest, Konkoly Thege Rd. 29-33, Hungary*
[3]*HORIBA Scientific, HORIBA Jobin Yvon S.A.S., Avenue de la Vauve - Passage Jobin Yvon, CS 45002 - 91120 Palaiseau – France*
[4]*Institute of Microwave and photonics, Electronic and Electrical Engineering, Faculty of Engineering, University of Leeds, LS2 9JT, UK*
*pmcj@leeds.ac.uk

Abstract: The limited solubility of rare-earths in silica hampers the development of loss-compensated photonic integrated circuits. We report a novel method using femtosecond laser plasma assisted hybrid material integration of rare-earth-doped tellurite with silica, achieving high doping concentration of Er^{3+} and Yb^{3+}-ions, 1.63×10^{21} atoms.cm^{-3}, without segregation validated by Er^{3+}:$^4I_{13/2}$ lifetime of 9.1 ms. The sequential ablation of two individual rare-earth (Er^{3+}/Yb^{3+}) doped-tellurite glass targets produces an exceptional intermixing of Er^{3+} and Yb^{3+}-ions extending to the pristine silica with sharp interface. Formation of such homogeneous glass structure with Er^{3+}-Yb^{3+}-ions in a matrix of silica is not possible to realise by conventional methods.

References and links

1. H. Isshiki, F. Jing, T. Sato, T. Nakajima, and T. Kimura, "Rare earth silicates as gain media for silicon photonics [Invited]," Photonics Res. **2**(3), A45 (2014).
2. A. Kenyon, "Recent developments in rare-earth doped materials for optoelectronics," Prog. Quantum Electron. **26**(4-5), 225–284 (2002).
3. A. Polman, "Erbium implanted thin film photonic materials," J. Appl. Phys. **82**(1), 1 (1997).
4. F. Priolo, T. Gregorkiewicz, M. Galli, and T. F. Krauss, "Silicon nanostructures for photonics and photovoltaics," Nat. Nanotechnol. **9**(1), 19–32 (2014).
5. M. J. R. Heck, J. F. Bauters, M. L. Davenport, J. K. Doylend, S. Jain, G. Kurczveil, S. Srinivasan, and J. E. Bowers, "Hybrid silicon photonic integrated circuit technology," IEEE J. Sel. Top. Quantum Electron. **19**(4), 6100117 (2013).
6. G. C. Righini and A. Chiappini, "Glass optical waveguides: a review of fabrication techniques," Opt. Eng. **53**(7), 071819 (2014).
7. Y. Arakawa, T. Nakamura, Y. Urino, and T. Fujita, "Silicon photonics for next generation system integration platform," IEEE Commun. Mag. **51**(3), 72–77 (2013).
8. F. Auzel and P. Goldner, "Towards rare-earth clustering control in doped glasses," Opt. Mater. (Amst) **16**(1-2), 93–103 (2001).
9. L. Yin, H. Ning, S. Turkdogan, Z. Liu, P. L. Nichols, and C. Z. Ning, "Long lifetime, high density single-crystal erbium compound nanowires as a high optical gain material," Appl. Phys. Lett. **100**(24), 241905 (2012).
10. A. Amarnath Reddy, S. Surendra Babu, and G. Vijaya Prakash, "Er^{3+}-doped phosphate glasses with improved gain characteristics for broadband optical amplifiers," Opt. Commun. **285**(24), 5364–5367 (2012).
11. G. C. Righini and M. Ferrari, "Photoluminescence of rare-earth – doped glasses," Riv. DEL NUOVO Cim. **28**, 1–53 (2006).
12. E. Snoeks, P. G. Kik, and A. Polman, "Concentration quenching in erbium implanted alkali silicate glasses," Opt. Mater. (Amst) **5**(3), 159–167 (1996).

13. G. Jose, T. T. Fernandez, D. Steenson, and A. Jha, "Multi-ion diffusion in silica glass using femtosecond pulsed laser deposition," Conf. Lasers Electro-Optics 2012 CM3L.6 (2012).
14. J. Chandrappan, M. Murray, T. Kakkar, P. Petrik, E. Agocs, Z. Zolnai, D. P. Steenson, A. Jha, and G. Jose, "Target dependent femtosecond laser plasma implantation dynamics in enabling silica for high density erbium doping," Sci. Rep. **5**, 14037 (2015).
15. A. Jha, B. D. O. Richards, G. Jose, T. Toney Fernandez, C. J. Hill, J. Lousteau, and P. Joshi, "Review on structural, thermal, optical and spectroscopic properties of tellurium oxide based glasses for fibre optic and waveguide applications," Int. Mater. Rev. **57**(6), 357–382 (2012).
16. Z. Zolnai, N. Nagy, A. Deák, G. Battistig, and E. Kótai, "Three-dimensional view of the shape, size, and atomic composition of ordered nanostructures by Rutherford backscattering spectrometry," Phys. Rev. B **83**(23), 233302 (2011).
17. Z. Zolnai, M. Toporkov, J. Volk, D. O. Demchenko, S. Okur, Z. Szabó, Ü. Özgür, H. Morkoç, V. Avrutin, and E. Kótai, "Nondestructive atomic compositional analysis of BeMgZnO quaternary alloys using ion beam analytical techniques," Appl. Surf. Sci. **327**, 43–50 (2015).
18. F. Pászti, A. Manuaba, C. Hajdu, A. A. Melo, and M. F. Da Silva, "Current measurement on MeV energy ion beams," Nucl. Instruments Methods Phys. Res. Sect. B Beam Interact. Mater., Atoms **47**, 187–192 (1990).
19. E. Szilágyi, F. Pászti, and G. Amsel, "Theoretical approximations for depth resolution calculations in IBA methods," Nucl. Instruments Methods Phys. Res. Sect. B Beam Interact. Mater., Atoms **100**, 103–121 (1995).
20. E. Kótai, "Computer methods for analysis and simulation of RBS and ERDA spectra," Nucl. Instruments Methods Phys. Res. Sect. B Beam Interact. with Mater, Atoms **85**, 588–596 (1994).
21. A. Tempez, S. Legendre, and P. Chapon, "Depth profile analysis by plasma profiling time of flight mass spectrometry," Nucl. Instruments Methods Phys. Res. Sect. B Beam Interact. Mater., Atoms **332**, 351–354 (2014).
22. S. W. Schmitt, C. Venzago, B. Hoffmann, V. Sivakov, T. Hofmann, J. Michler, S. Christiansen, and G. Gamez, "Glow discharge techniques in the chemical analysis of photovoltaic materials," Prog. Photovolt. Res. Appl. **22**(3), 371–382 (2014).
23. N. Da, A. A. Enany, N. Granzow, M. A. Schmidt, P. S. J. Russell, and L. Wondraczek, "Interfacial reactions between tellurite melts and silica during the production of microstructured optical devices," J. Non-Cryst. Solids **357**(6), 1558–1563 (2011).
24. R. Hellmann, S. Cotte, E. Cadel, S. Malladi, L. S. Karlsson, S. Lozano-Perez, M. Cabié, and A. Seyeux, "Nanometre-scale evidence for interfacial dissolution-reprecipitation control of silicate glass corrosion," Nat. Mater. **14**(3), 307–311 (2015).
25. E. G. Gamaly, A. V. Rode, B. Luther-Davies, and V. T. Tikhonchuk, "Ablation of solids by femtosecond lasers: Ablation mechanism and ablation thresholds for metals and dielectrics," Phys. Plasmas **9**(3), 949 (2002).
26. A. Muhammad Noorazlan, H. Mohamed Kamari, S. S. Zulkefly, and D. W. Mohamad, "Effect of Erbium Nanoparticles on Optical Properties of Zinc Borotellurite Glass System," J. Nanomater. **2013**, 1–8 (2013).
27. C. Eggeling, J. R. Fries, L. Brand, R. Günther, and C. A. Seidel, "Monitoring conformational dynamics of a single molecule by selective fluorescence spectroscopy," Proc. Natl. Acad. Sci. U.S.A. **95**(4), 1556–1561 (1998).

1. Introduction

Rare-earth (RE) doped silicates have been widely explored as an amplifying medium for the optical communication systems [1]. The intra-4f transition $^4I_{13/2} \rightarrow {}^4I_{15/2}$ in erbium (Er^{3+}) ions matches the C + L-band communication wavelength (1530-1605 nm), which makes them attractive for optical amplifier and laser applications [2]. In erbium doped fiber amplifiers (EDFAs), long lengths of fibers (>5 m) are required to achieve more than 20dB gain, this long length requirement is due to the limited solubility of Er^{3+}-ions in silica [3]. On the other hand, the advances in integrated optics and silicon photonics favor miniaturized optoelectronic devices including the optical amplifiers where the fiber-based amplification geometry is undesirable [4,5]. Furthermore, on-chip integration of both passive and active photonic components is preferred to achieve highly dense optical interconnects. However, such complex multi-level integration demands loss compensating devices to eliminate the optical power losses associated with multi-channel array waveguides, optical power splitters and de-multiplexers [6]. The loss-compensated devices can promote cost-effective optical integrations by engaging ultra-low power optical transmitters and economical receivers in the communication network. In this respect high-gain, erbium-doped waveguide amplifiers are necessary to overcome the signal degradation and realize the future system in package (SiP) solutions [7].

Lack of a suitable optical material platform, for fabricating large gain per unit length amplifiers, is limiting the development of multifunctional photonic integrated circuits. The chemical limitations of RE ion solubility in pure silica (0.7×10^{18} cm^{-3}) can be improved by using phosphate and tellurite glass substrates platforms in which high doping concentrations

up to 2.2×10^{21} cm^{-3} is possible to achieve [8]. Nevertheless, even such a high concentration of RE ions in phosphate and tellurite hosts has not yet yielded a suitable optical gain medium. Recently reported erbium chloride incorporated silicates can have Er^{3+}-ion density of 10^{22} cm^{-3}, but the metastable lifetime is 20 times shorter at 540 μs than in standard EDFA [9]. This shortened lifetime is due to the phenomena of concentration quenching, where the physical limits of ion-ion interactions are reached, assisting macroscopic energy transfer, evidenced by the very short lifetimes at the $^4I_{13/2}$ level [10, 11].

Given the choice of materials, silica holds the advantage of CMOS process compatibility, and erbium-doped silicate waveguides (EDSW) have the potential to develop CMOS-photonic integrated circuits to the next level of complex photonic integrations. However, the on-chip amplification places great challenges on EDSW development as the optical gain is related directly to the erbium concentration and the waveguide dimensions. To meet the needs for CMOS-photonic integrated circuits, and the underpinning role of an Er^{3+}-ion based amplification strategy, the only way a significant breakthrough may arise is if Er^{3+}-ions are incorporated into the silica substrate at much higher concentrations ($\geq 10^{20}$ cm^{-3}), without concentration quenching and shortening of the metastable lifetime at $^4I_{13/2}$ level [9]. In addition, the amplification medium must be able to incorporate Yb^{3+}-ion for enhancing pump absorption via $^2F_{7/2} \rightarrow {}^2F_{5/2}$ over a short distance. The co-doping of Yb^{3+}-ion allows the efficient inversion of Er^{3+}-ions via resonant energy transfer from $Yb^{3+}:{}^2F_{5/2} \rightarrow Er^{3+}:{}^4I_{13/2}$, and assist in increasing the mean inter-atomic distance to minimize the Er^{3+}-ion energy transfer interactions [11].

For achieving such a challenging goal, none of the standard fabrication techniques are likely to yield the desirable spectroscopic performance [12]. Innovative fabrication methods are necessary to tackle the challenges related to the chemical and physical limits of high RE concentrations in silica. A multi-element doping in oxygen rich environment containing silica glass modifiers and silicate glass formers might be beneficial to change the scenario vividly. Hence, we propose an alternative technique, based on ultrafast laser plasma assisted RE-rich tellurite and silica hybrid material integration, to enhance the RE solubility and photoluminescence (PL) emission characteristics of REs in silica. In this technique, multi-ion doping, including Er^{3+}-ions, is possible into the silica glass network [13]. The technique allows us to transcend thermodynamic barriers to achieve unique compositions, which otherwise is impossible to fabricate via conventional methods. The modified silica layer thickness and PL lifetimes can be precisely controlled by process parameters, as shown elsewhere [14].

In this article, we demonstrate an unusual RE ion (Yb^{3+} and Er^{3+}) mixing in the silicate matrix during fs laser-induced plasma assisted sequential doping process that make a significant step change in dopant incorporation process into a silica substrate for planar waveguide amplifier engineering. A single co-doped Er^{3+}-Yb^{3+}-tellurite target glass was also used for comparison. The former method enhances both the modified silicate layer thickness and PL characteristics, as compared to the doping of Er^{3+}/Yb^{3+}-ions co-doped tellurite into silica. The results of inter-layer mixing yields remarkable spectroscopic results and shall eliminate the issues related to the fabrication of dense Er^{3+}-doped silica platform.

2. Experimental

Tellurite glass targets of molar percentage concentrations (a) $79TeO_2$-$10ZnO$-$10Na_2O$-$1Er_2O_3$ (TZN-Er), (b) $79TeO_2$-$10ZnO$-$10Na_2O$-$1Yb_2O_3$ (TZN-Yb) and (c) $78TeO_2$-$10ZnO$-$10Na_2O$-$1Er_2O_3$-$1Yb_2O_3$ (TZN-Er-Yb) were prepared using standard glass melting and quenching processes [15]. The fs laser plasma assisted doping process was carried out in a vacuum chamber under an oxygen (O_2) atmosphere of 80 mTorr and at an optimum processing temperature of 973 K. A laser source with a pulse duration of 100 fs, operation wavelength of 800 nm, pulse repetition rate of 1 kHz and single pulse energy of 50 μJ was used to ablate the targets. The silica glass substrate, measuring $30 \times 20 \times 1$ mm (width × length × thickness),

was positioned 70 mm above and parallel to the tellurite target for receiving the ablated high energy plasma plumes.
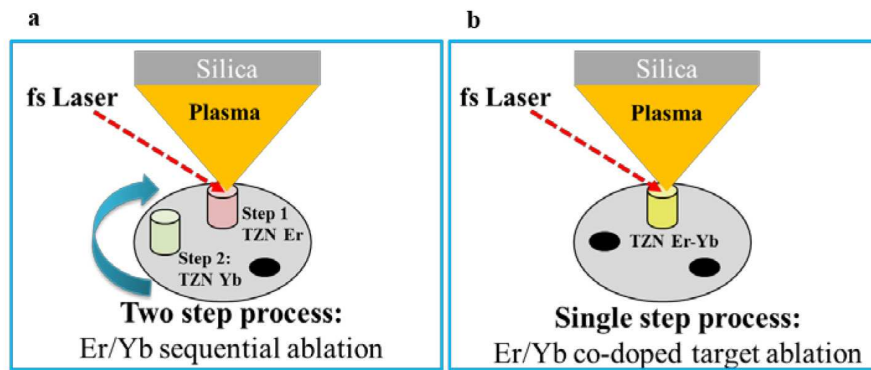

Fig. 1. Schematic of the procedural differences in the fabrication of Er^{3+}-Yb^{3+}-tellurite modified silica layers. (a) Illustrate the sequential ablation and doping of Er^{3+} and Yb^{3+} tellurites into silica using a two-step process. (b) Conventional single step process of Er^{3+} and Yb^{3+} co-doped target ablation and doping.

Individual process sequences are illustrated in Fig. 1. The sequential approach was used to prepare sample 1 (S1), initiated by the ablation of the target TZN-Er first for 2 hours and then instantaneously continued with the second target TZN-Yb for the following 2 hours without changing the ambient conditions. Sample 2 (S2) used a TZN-Er-Yb, single co-doped target, continuously ablated for 4 hours under the identical process conditions.

The structural characterization was done using transmission electron microscopy (TEM) FEI Tecnai TF20 field emission gun (FEG) TEM (200 kV) fitted with a high angle annular dark field (HAADF) detector; a Gatan SC600 Orius CCD camera (Gatan Inc., Pleasanton, CA); and an Oxford Instruments 80 mm^2 X-max SDD energy dispersive X-ray spectroscopy (EDX) detector (Oxford Instruments plc, Abingdon, UK). Rutherford Backscattering Spectrometry (RBS) is a powerful technique for non-destructive compositional analysis of thin layers and nanostructured materials [16, 17]. In this work, RBS analysis was performed in a scattering chamber with a two-axis goniometer connected to the 5 MV EG-2R Van de Graaff accelerator of the Institute for Particle and Nuclear Physics at the Wigner Research Centre for Physics (Wigner FK RMI) in Budapest, Hungary. The 2820 keV $^4He^+$ analyzing ion beam was collimated with two sets of four-sector slits to the spot size of 0.5×0.5 mm^2 while the beam divergence was kept below 0.06°. The beam current was measured by a transmission Faraday cup [18]. Backscattering spectra were detected using an ORTEC surface barrier detector mounted in Cornell geometry – detector under the beam, with vertical sample rotation axis – at scattering angle of $\Theta = 165°$. An electron source installed in the sample chamber was used to avoid ion beam-induced charging of the insulating glass samples. In the spectrum recording, a blind detector with a thin Aluminium reflection layer on top was used to prevent light-induced background counts originating from the electron source and ion beam induced luminescence of the glass samples. The energy resolution of the detection system was 20 keV. Note, in this work the depth resolution of RBS at the sample surface is about 3 nm, and poorer values can be considered as a function of depth [19]. Spectra were recorded for sample tilt angles of 7° and 45°. The RBX spectrum simulation has been performed to achieve best fits simultaneously for both tilt angles. The measured data were evaluated with the RBX spectrum simulation code [20]. The effective thickness of the modified layers was estimated supposing an atomic layer density of silicon dioxide, $N = 6.5 \times 10^{22}$ atom cm^{-3}. This value can be calculated from silica glass density measurements resulting in 2.2 g/cm^3. The relative elemental concentrations in the samples were obtained using plasma profiling time of flight mass spectrometry (PP-TOFMS) by Horiba Scientific, France [21]. PP-TOFMS

combines a glow discharge (GD) plasma and an orthogonal time of flight mass spectrometer. The plasma is created in ultra-pure Argon between a grounded electrode and the sample, which is powered from its back with a pulsed 13.56 MHz RF voltage. The plasma ensures fast and uniform material removal over a 4 mm diameter area from the surface to the bulk and parallel excitation/ionization of the sputtered species. The ultrafast and full mass coverage TOFMS detection is adapted to the fast erosion rate (up to tens of nm/s) of the plasma. Time of Flight (TOF) records a full and continuous mass spectrum in every 30 μs, thereby providing constant monitoring of all the species throughout the depth profile. An instantaneous semi-quantification giving elemental atomic concentrations can be obtained by calculation of Ion Beam Ratios (IBR). The IBR approach is commonly used in glow-discharge mass spectrometry (GDMS). It is based on calculating the ratio of ion current for any one isotope with respect to the total ion current except the signal rising from the plasma gas and using the assumption that this ratio is representative of the atomic concentration of that isotope in the sample [22]. A Metricon Model 2010 prism coupler at 1550 nm was used to measure the planar optical layer thickness and refractive indices on the silica substrate. The amplitude ratio (Ψ) and phase difference (Δ) of the complex reflectance ratios for light polarized parallel and perpendicular to the plane of incidence were measured using a Woollam M-2000DI rotating compensator spectroscopic ellipsometer at the Institute for Technical Physics and Materials Science in Budapest, Hungary. The optical properties of each sub-layer were calculated using the Cauchy dispersion of $n = A + B/\lambda^2 + C/\lambda^4$ (where λ denotes the wavelength and A, B and C denote the Cauchy parameters) and the Urbach dispersion of $k = D*e^{E\lambda}$ (where E and D are the Urbach parameters). The optical properties of the substrates were measured on the polished backside of the samples. The parameters of B and C were fixed at the values of the substrate, whereas parameter E was fixed at the value of the highest absorption surface layer, fitting the UV part of the spectrum with the smallest penetration depth. Consequently, only parameters A and D were fitted, resulting in acceptably low uncertainties. Typical uncertainties of A and D are 10^{-3} and 10^{-1} in the near surface and bottom interface regions, respectively. Acquisition of the transmission spectra for these samples was done using PerkinElmer LAMBDA 950 UV/Vis/NIR spectrophotometer. Standard excitation and emission fluorescence of the rare-earth doped silicate samples were obtained using an Edinburgh Instruments FLS920 series of spectrometer. FLS920 is fitted with liquid nitrogen cooled photomultiplier tube (PMT) near-infrared (NIR) detector, operating in the 700-1700 nm wavelength range and a JDSU pump laser source operating at a wavelength of 980 nm, respectively. The fluorescence lifetime was also calculated using a time-resolved fluorescence spectra, whereby the laser source was pulsed with a 100 ms period and a pulse width of 10 μs.

3. Results and discussion

3.1 Material characterization

The high-resolution TEM cross-sectional images of the samples S1 and S2, as prepared by focused ion beam (FIB) lithography is shown in Fig. 2(a) and 2(b), respectively. Both sequential and single step doping process, described above, result in a homogenous metastable state of rare-earth doped tellurite modified silica (RETS). The sharp interface between the RETS and pristine silica attained through these processes is shown in Fig. 2(c) at high magnification.

The accompanying selected area electron diffraction (SAED) patterns, shown in Fig. 3, demonstrate a typical amorphous nature of both the RETS region and the pristine substrate, respectively, showing a lack of long-range order in the atomic lattice, and exhibiting diffuse ring diffraction patterns without any discrete reflections. Note the difference in the sizes of diffraction rings in Fig. 3 for the RETS layer and pristine silica, respectively. It can be clearly seen that the ring radius of the SAED pattern from the RETS layer is larger than in the pristine silica region. It is known that the radius of the ring is inversely proportional to the corresponding inter-atomic spacing in the sample. The average spatial distribution of atoms

calculated from the ring radius for the modified site of sample S1 is 1.35 A°, 27% shorter than the pristine silica, measuring 1.86 A°. The shorter spacing indicates that the RETS layer is more closely packed, and therefore of greater density, than the base silica layer. The dense packing is due to the modification of the silica network with heavier tellurium and RE ions. The RETS layer formed by the sequential approach was further analyzed using energy dispersive X-ray spectroscopy (EDX). Mapping scans of 1.4 µm thick sample, prepared similar to S1, in Fig. 4 reveals the generation of a uniform, homogenous mixture of Er^{3+} and Yb^{3+} extending to the bottom of the modified layer.
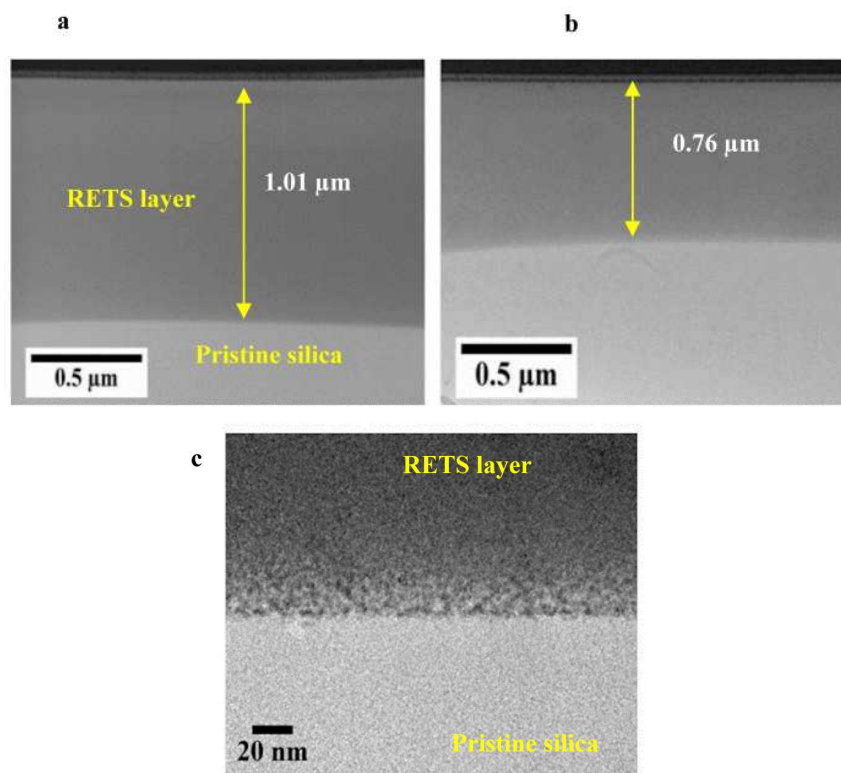

Fig. 2. High-magnification TEM image of the RETS layer formed under identical conditions by (a) Sequential ablation of individual Er^{3+}/Yb^{3+}-doped tellurites, sample S1. (b) Single target ablation of Er^{3+} and Yb^{3+} co-doped tellurite, sample S2. (c) High angle annular dark field (HAADF) cross-sectional image of S1 showing the interface of pristine silica and RETS.

Sample S1 was characterized by plasma profiling time of flight mass spectrometry (PP-TOFMS) for semi-quantification of the element concentrations. It can be seen from Fig. 5 that the tellurite compounds along with RE elements are mixed well with silica and the modified layer extends to the pristine silica region. A silica-rich RETS layer with homogeneously distributed Er and Yb is obtained, irrespective of the sequential ablation. There exists a cross-over point (interfacial region) where the RETS layer profile gradually transits to the pristine silica. A more precise quantification to obtain the concentration profile was attempted here by calculating the correction factors or relative sensitivity factor using the known composition of the target containing Er^{3+}/Yb^{3+} to correct for elemental variation in analytical sensitivity (as a result of different ionization cross sections and transmission efficiencies). An error of about 30% (higher for Te) is expected, as the reference sample was not fully 'matrix matched' to the RETS layer (i.e. it does not include Si in the target glass). So currently the PP-TOFMS analysis is used here to obtain the distribution profile of elements, especially to validate the homogenous mixing of Er and Yb in RETS layer.
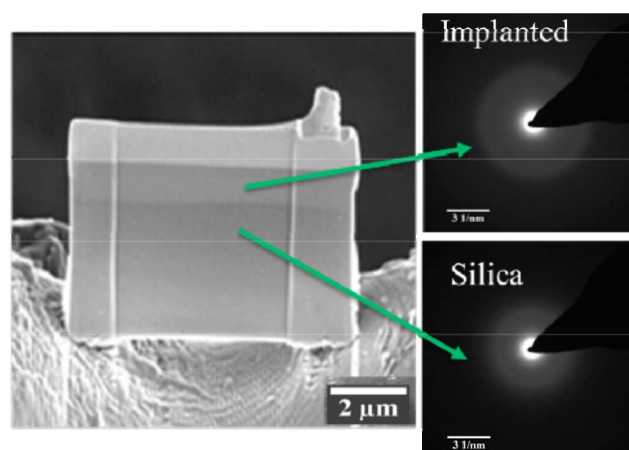
Fig. 3. SAED pattern from the modified RETS layer and pristine silica region from sample S1. The larger diffraction ring radius of the modified layer implies higher density compared to the pristine silica layer.
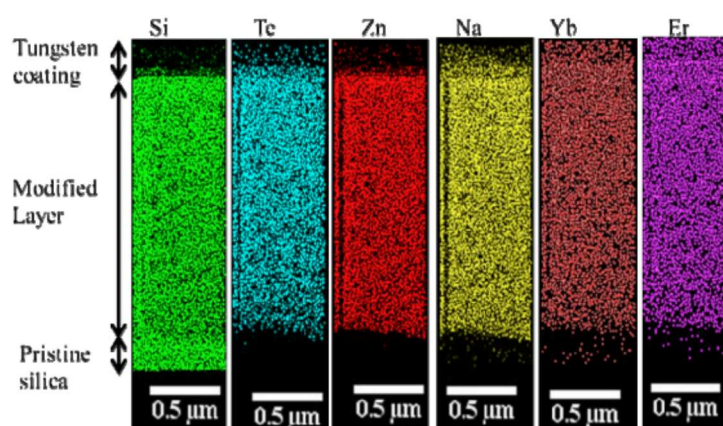

Fig. 4. EDX mapping acquired during cross-sectional TEM analysis of a 1.4 μm thick sample prepared by the sequential approach (similar to S1). The distribution of various elements in the RETS layer is indicated. Homogenous mixing of Er and Yb is achieved irrespective of the sequential doping.
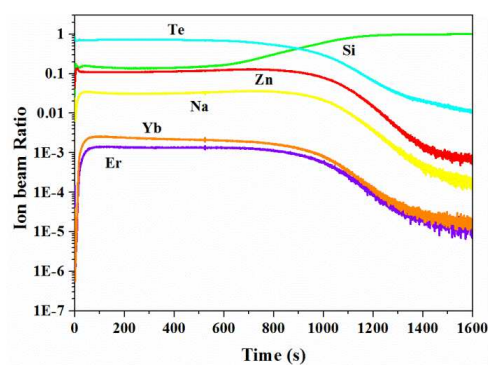

Fig. 5. PP-TOFMS profile of sample S1. Ion beam ratio of the elements in the sample indicating the uniform distribution of Er and Yb

Based on the EDX mapping and the PP-TOFMS findings, the process can be assumed to be controlled by both highly energetic ions in the laser plasma and the high process temperature, 973K (below the glass transition temperature of silica), that initiates an interfacial reaction between the ablated target glass material and the silica substrate. Above 873 K, the alkali metals in the compound (Te and Na) attack the silica substrate, enabling the regular dissolution of silica throughout the process and results in the formation of a well-defined metastable homogeneous modified RETS layer [23, 24]. A similar phenomenon is also observed for the subsequent ablated target material, in which significant intermixing between the second layer (Yb^{3+}-doped) and the first layer (Er^{3+}-doped) arises. Consequently a uniform distribution of Er^{3+} and Yb^{3+}-ions in the single modified layer becomes apparent, as can be seen from the elemental maps in Fig. 4. The evidence implies that even though the Er^{3+} and Yb^{3+}-doped tellurites were ablated sequentially, interfacial reactions and intermixing of the layers help the Yb^{3+}-doped layer to extend down to the modified-pristine silica boundary, suggesting that over a period of two hours, sufficient ion mobility may be occurring during the process at 973K. Such novel nanoscale layer formation, without silica precipitation, is not possible with conventional fabrication methods, and this represents a step-change in materials production.
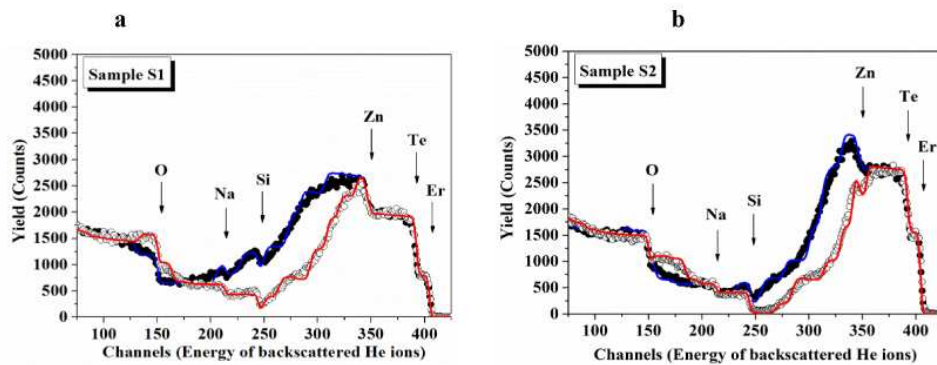

Fig. 6. RBS spectra of the implanted layer/SiO_2 substrate measured at two different sample tilt angles of 7° (open dots) and 45° (solid dots), respectively. The corresponding RBX simulations are also shown (red and blue lines). Surface spectrum edges for Er, Te, Zn, Si, Na and O are indicated. (a) Sample S1, (b) Sample S2.

RBS spectra of both samples, S1 and S2, were taken to estimate the atomic composition for O, Si, Na, Zn, Te, and Er/Yb. The sample spectra, S1 and S2, along with their simulations are shown in Fig. 6(a) and 6(b), respectively. RBS cannot distinguish between Er and Yb due to their very similar energy threshold, so the peak corresponding to Er in the RBS spectra indicate both Yb and Er content together. In Fig. 6(a), the different height of the spectra at channel numbers above 250 is primarily due to the different Er/Yb content. For S2, nearly the double height of the Er shoulder can be observed than for S1, revealing about two times higher Er/Yb concentration. The spectrum S1 is significantly wider as it can be observed for the Zn, Te, and Er components (Na and O overlap with the substrate SiO_2 signal). This broad spectrum is the consequence of the thicker modified silica layer for sample S1. The atomic composition and evaluated effective layer thicknesses are summarized in Table 1. The depth profiles with atomic concentrations of various elements as evaluated from the RBS spectra using a simple two-layer model are represented in Fig. 7(a) and 7(b).

Table 1. Parameters used in the RBX simulation of the measured RBS spectra. Effective thicknesses of the implanted layers given in nm are recalculated from thicknesses given in atom/cm^2 (provided by the RBS analysis) assuming the atomic density of silica, respectively. The estimated uncertainty of the evaluated Er contents is ± 0.05 at. %.

Target glass composition (mol.%)	Sample	Implanted layer composition (at. %)						Implanted layer effective thickness (nm)	Transition layer effective thickness (nm)
		Si	O	Er (+Yb)	Te	Zn	Na		
79.0TeO$_2$-10ZnO-10Na$_2$O-1Er$_2$O$_3$ /1Yb$_2$O$_3$	**S1**	18	56.9	1.45	3.5	6.4	13.7	820	~185
78.0TeO$_2$-10ZnO-10Na$_2$O-1Er$_2$O$_3$ -1Yb$_2$O$_3$	**S2**	17	60	2.8	3.6	5.8	10.8	633	153

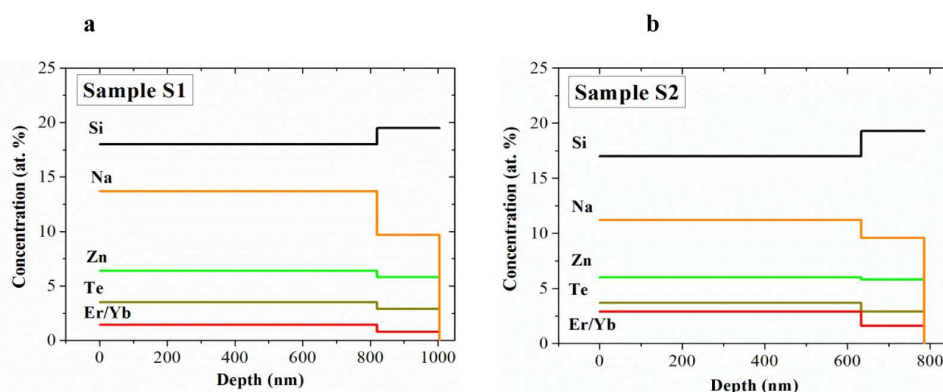a   b

Fig. 7. Atomic concentrations vs. depth in the implanted layer as evaluated from 2.82 MeV He$^+$ RBS spectra using a simple two layer model. (a) Sample S1, (b) Sample S2.

The effective doping concentration of Er and Yb in sample S1 and S2 is 1.45 at. % (0.89 × 10^{21} cm^{-3}) and 2.8 at. % (1.63 × 10^{21} cm^{-3}), respectively. Notably, this is the highest ever reported RE doping concentration in pure silica, without RE clustering, to the best of our knowledge [2, 9].

It is observed that the RE content in sample S1 is almost 50% of Sample S2. This change is related to the individual target ablations time (2 Hrs.) in the preparation of S1 which is exactly half of the co-doped target ablation time (4 Hrs.) for the preparation of S2. The amount of RE in S1 can be improved by increasing the processing time that will further help to increase the thickness of RETS layer whereby maintaining the larger spacing between the doped ions.

The increased concentration of RE dopants in silica might change the structural packing environment and require more oxygen per mole of RE to form a stable compound. This RE concentration increase could be the reason for the oxygen atomic composition variation for S1 and S2 as reflected in the data shown in Table 1.

3.2 Optical characterization

The RETS layers were analyzed for their planar optical layer characteristics using the prism coupler. The layer thickness and refractive indices were obtained at a wavelength of 1550 nm. The planar optical layer thickness for S1 is 1.01 μm, while S2 measures 0.76 μm with refractive indices of 1.592 and 1.610, respectively. For a similar overall processing time, a 30% higher thickness is observed with the two target sequential approach than the single co-doped rare-earth target case, while the refractive index of the single target process is greater

than the two target process. Figure 8(a) indicates the typical refractive index profile of 1.4 µm RETS layer fabricated through the femtosecond (fs) laser plasma-assisted process. The data reveals the formation of a uniform layer of step index waveguide with a refractive index of 1.6 on silica at a wavelength of 1550 nm.

The refractive index (n) and extinction coefficient (k) profiles have been further calculated using multi-layer optical models using the ellipsometric data. Figure 8(b) shows typically measured and fitted ellipsometric spectra and the depth profiles of the optical properties (in the inset) calculated from the fit.
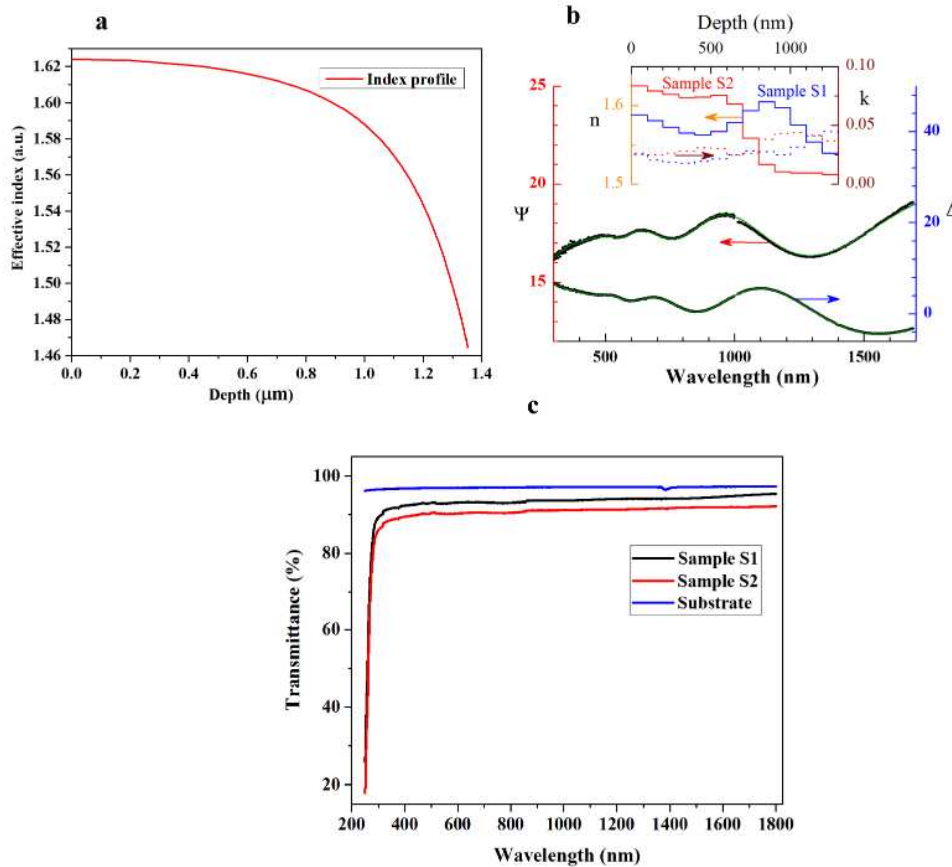
Fig. 8. (a) Typical step index profile of RETS layer characterized at a wavelength of 1550 nm. (b) Measured (black dots) and fitted (solid lines) ellipsometric spectra at an angle of incidence of 70° for sample S2; The inset shows the depth profiles of the refractive index (solid curve) and extinction coefficient (k, dotted line) at the wavelength of 1550 nm for S1 and S2, calculated from the fit. (c) The UV-Vis-NIR transmittance of the substrate and the samples, S1 and S2.

As seen from the above optical characterization of the RETS layer, sample S1 compared to the sample S2 is higher in thickness and lower in refractive index with similar k values. The drop in thickness and the increased refractive index can be ascribed to the RE concentration in the tellurite target glass and hence in the implanted film. The relative concentration of RE is higher in the co-doped single target compared to the dual target composition. The replacement of Tellurium (Te) with heavier RE atoms gives rise to the density of the target glass, measured using Accupyc 1330 Pycnometer, as indicated in Fig. 9. It can be assumed that the ablation rates for the dense materials are comparatively lower [25],

at a fixed fs laser energy, leading to a drop in the level of ablated materials reaching the surface of the silica substrate. Again the reduced Te (alkali metal) content in the ablated material can slow down the interfacial reactions with silica and its dissolution (validated with RBS data, Si at.% for S1 ~18, S2 ~17), decreasing the rate of formation of the RETS layer and hence the thickness drops. The addition of rare-earth-tellurites results in a denser packing of ions in the silica network as shown by the SAED pattern and the refractive index, which is directly linked to the material density. Sample S1 contains lower RE content (1.45 at. %) compared to S2 (2.8 at. %), and the increase of highly polarized trivalent Er^{3+}-ions will generate more non-bridging oxygen in glass networks, and the polarizability of the material increases, thus increasing the refractive index [26].

The UV-Vis-NIR transmittance of each sample is obtained and presented in Fig. 8(c).The transmittance of the substrate is also included in Fig. 8(c) for reference. The variations of transmittance with wavelength were comparable for the samples, giving sample S1 the high value of 95% in the C-band wavelength range. The changes in the transmittance are minimal which can be attributed to the differences in their refractive index and the absorption characteristics of the RETS layer. The optical absorption characteristics are greatly affected by the oxygen bond strength related to the structural changes in the glass system with the addition of Er^{3+}-ions. It is obvious that the bond strength depends on the concentration and the oxide state of the glass network modifier ions [26]. Accurate values of the propagation losses that translate into waveguide losses shall be measured as part of further investigations.
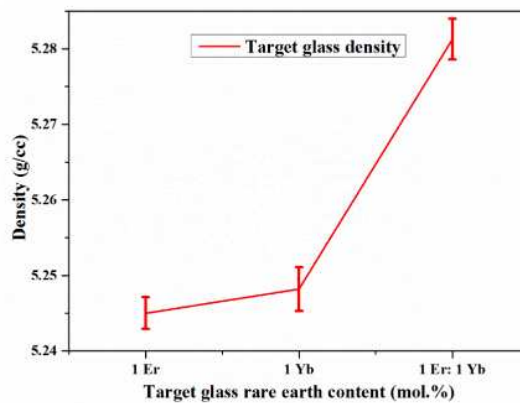

Fig. 9. Typical density variation of Tellurite target glass with RE concentration.

The steady-state PL emission characteristics were obtained by exciting the glass samples with a pump source at 30 mW of output power. Under the same experimental conditions, the spectral emission range was scanned from 1400 to 1700 nm with a resolution of 0.5 nm. The PL spectra for both samples, corresponding to the $^4I_{13/2} \rightarrow {}^4I_{15/2}$ transition in Er^{3+}-ion, are presented in Fig. 10(a). The figure also displays the PL spectrum of 1 mol.% Er^{3+}-doped (no co-doped Yb^{3+}) silica fabricated and characterized under similar conditions. This spectrum is to provide a comparison and the evidence of direct Yb to Er energy transfer that accounts for the strong emissions from the co-doped samples S1 and S2. The PL emission intensity appears comparable between the two processing strategies, with lower peak intensity for the sample S2, prepared using the single target approach. The lifetime of the sample S1, prepared with the sequential ablation process was, 12.94 ms, while the co-doped single target sample S2 was 9.16 ms as shown in Fig. 10(b). Both samples demonstrate spectroscopic properties that are superior to the state of the art [9]. The reduced PL intensity and lifetime in sample S2 are likely to be due to the relatively higher concentration of Er^{3+}-ions, leading to concentration quenching of the transition. The increased concentrations of RE ions decrease

the ion spacing to a level where the dipole-dipole interactions between the Er^{3+}-ions are prominent, and energy migration occurs. Furthermore, the higher erbium concentration creates a relatively larger polar environment, validated by the higher refractive index of the sample S2. The fluorescence lifetime tends to be shorter in the more polar environment as the system tries to stabilize as quickly as possible from the excited level by radiative emissions [27].
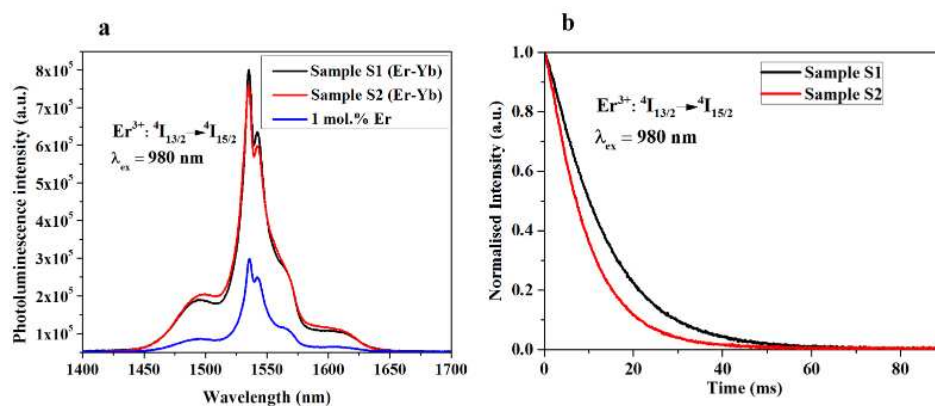

Fig. 10. Comparison of the PL emission characteristics of the RETS samples fabricated using single co-doped target and sequential two targets. (a) PL intensity profile shows comparable performance for both S1 and S2. Luminescence spectrum of erbium-doped silica is also shown in comparison to the co-doped samples. (b) Fluorescence lifetime profile measuring lifetime of 12.94 ms for sample S1 compared to 9.16 ms for S2.

4. Conclusions

In summary, high doping levels of Yb^{3+} sensitized Er^{3+}-ions have been demonstrated in silica without crystallization, through fs laser plasma assisted hybrid integration of RE ion enriched tellurite target glass and silica. The highly energetic ions in the fs laser plasma and the high substrate temperature enable the formation of a metastable RETS layer. The higher oxygen content in the RETS network ensures stable oxide formation, which is a pre-requisite for improved fluorescence efficiency. We observe substantial RE doping concentrations of 1.63×10^{21} atoms/cm^3, for the current set of experimental data and could be further improved by using higher doping concentration of RE in the target glass. Such high RE doping demonstrates the prime applicability of this fabrication technology for the progress of planar optical amplifiers, which we perceive to be unsurpassable through current alternatives due to the unique material characteristics.

The proper interlayer mixing accomplished the effective sensitization of Er^{3+} with Yb^{3+}-ions, even when sequentially ablating these ions from two individual targets. This unique method opens up a new horizon of knowledge in doping of Er^{3+} and Yb^{3+}-ions in silica platform using fs laser plasma-assisted process. Indeed, the two target approach enhanced the RETS layer characteristics still further. This is attained by the lower RE concentrations of the target glass enabling a thicker RETS layer formation on silica for a given processing time [14]. Additionally, this aids in the realization of a homogeneous distribution of doped ions in larger average spacing, permitting higher doping concentration without significant fluorescence quenching. The comparable PL intensities indicate that the Yb^{3+}-ions are in close proximity to Er^{3+}-ions and the energy transfer is efficient, regardless of the sequential processing strategy presented here. The methodology also surpasses the co-doped target approach with a 35% longer PL lifetime which is highly beneficial for EDSWs. This method ensures homogeneously doped Er^{3+}-Yb^{3+} step index planar optical layers with high index contrast and enhanced thicknesses on a silica platform that strongly supports the development of loss compensated photonic integrated circuits.

Acknowledgments